NANO LETTERS

pubs.acs.org/NanoLett Letter

Silver-Loaded Titania-Based Metal–Organic Frameworks as a Platform for Silver Ion Release for Antibacterial Applications

Anca Mazare,*,† Wolfgang H. Goldmann,† Esra Kocak,† Benedict Osuagwu, Shanshan Qin, Ran Cao, and Patrik Schmuki*

Cite This: *Nano Lett.* 2025, 25, 12547–12553 Read Online

ACCESS | Metrics & More | Article Recommendations | Supporting Information

ABSTRACT: Conventional Ag-decorated TiO_2 coatings suffer from low adsorption capacity and burst release kinetics, limiting long-term antibacterial efficacy and risking cytotoxicity. An entirely different payload release approach can be based on metal–organic frameworks (MOFs), which offer tunable porosity, high surface area, and internal diffusion channels. Here, we report a thermally stabilized Ti-based MOF [NH_2-MIL-125(Ti)] functionalized with Ag^+ via reactive deposition, enabling high Ag loading (~14.7 wt %) and sustained release. Annealing at 250 °C enhances aqueous stability, allowing diffusion-governed Ag^+ delivery over >48 h, with 77% of the Ag still present in the MOF after a 24 h release. The system exhibits dose-dependent antibacterial activity in powders and comparable efficacy in coatings, with a more gradual release profile. This scalable platform is promising for long-acting coatings, wound interfaces, and implantable materials.

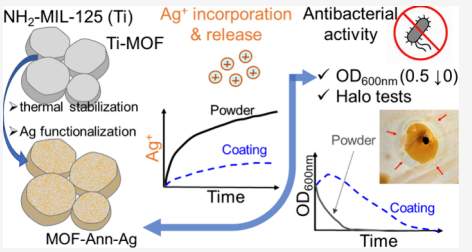

KEYWORDS: *metal–organic-frameworks (MOFs), NH_2-MIL-125, silver, antibacterial activity*

Titanium dioxide (TiO_2) nanostructures have been extensively studied for biomedical coatings due to their stability, biocompatibility, and antibacterial loading capacity.[1,2] A common strategy involves incorporating silver (Ag),[3] which exerts bactericidal effects by disrupting membranes, enzymatic interference, reactive oxygen species generation, and inhibition of protein synthesis and DNA replication.[4−7] Antibacterial delivery systems often lack controlled release, exhibiting burst profiles and limited adsorption sites, which result in transient activity and potential cytotoxicity.

Particularly, TiO_2 nanocavity structures such as nanotubes and wires offer a high surface area for Ag incorporation, but their rigid geometry and low internal porosity provide minimal control over release kinetics. As a result, their cumulative Ag^+ release is in the 0.4−3 mg·L^{-1} range over 2 weeks;[8] their nanometric geometry and rigidity lack internal diffusion pathways, often causing burst release. A significant part of the antibacterial element (e.g., Ag[8−10]) or drug is released in the first hours (up to 80% of the payload[11,12]), followed by a steep decline or a constant gradual zero-order kinetic release. This compromises the long-term efficacy and raises concerns about Ag toxicity. Especially in nanostructure reservoirs, a proper release trigger and valve must be established to prevent burst release (capping, decreased opening, etc.).

An entirely different payload release approach lies in metal–organic frameworks (MOFs): crystalline, porous materials featuring tunable porosity, modular chemistry, and high internal surface area. Applications include gas storage,[13] photocatalysis,[14,15] nuclear science,[16] and biomedical applications.[17−19] Therapeutic agent incorporation is achieved by coordination, encapsulation, or reactive infiltration. Titanium-based MOFs, such as NH_2-MIL-125(Ti), are particularly attractive for photocatalysis and antibacterial applications.[20,21] For the latter, their porous, diffusion-permissive architecture presents a fundamental advantage over other nanostructures, enabling defined incorporation and, conceptually, a gradual release of the payload (under physiological conditions). However, their poor aqueous stability due to ligand hydrolysis or displacement[22] hinders their use.

To overcome this, polymer coatings (polydopamine[21]) and thermal annealing[22] have enhanced the structural integrity, with the latter improving the stability of NH_2-MIL-125(Ti) in water,[22] yet its impact on Ag^+ incorporation and long-term release behavior remains unexplored.

Ag functionalization in MOFs strongly depends on Ag speciation, which governs the antibacterial efficacy. Two main classes are (1) Ag(I)-MOFs, with Ag^+ coordinated within the framework,[23−25] and (2) Ag@MOFs, with surface-bound silver nanoparticles (Ag^0 or AgBr).[26,27] While Ag(I)-MOFs allow gradual release (framework degradation), they often require complex ligands, limit scalability, provide slow or poorly controlled release profiles, and raise concerns over byproduct toxicity (degradation byproducts with unclear biological fate).

Received: May 19, 2025
Revised: July 3, 2025
Accepted: July 29, 2025
Published: August 7, 2025

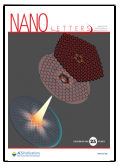

https://doi.org/10.1021/acs.nanolett.5c02681
Nano Lett. 2025, 25, 12547−12553

Ag@MOFs provide fast or stimulus-triggered Ag^+ release but lack dosing control and transient activity. Ag speciation is often ambiguous, with mixed Ag^+/Ag^0 states, complicating mechanistic understanding and hindering clinical translation. This makes it unclear whether the active species is Ag^+, Ag^0, or both.

In this work, we report a thermally stabilized NH_2-MIL-125(Ti) system functionalized with Ag as a hybrid framework for sustained Ag^+ delivery. The MOF primarily incorporates ionic Ag, and mild annealing enhances its aqueous stability. The resulting material exhibits a moderate initial release, followed by diffusion-governed Ag^+ delivery, making it suitable for long-acting antibacterial applications. Ag-MOF powders exhibit strong, dose-dependent antibacterial activity against *Escherichia coli*, while coatings on fluorine-doped tin oxide (FTO) show similar efficacy with slower release, highlighting their versatility for topical and surface-integrated use. With high Ag loading, scalable synthesis, and sustained efficacy, this platform holds strong potential for biomedical applications, including antimicrobial coatings, wound interfaces, and hybrid scaffolds requiring controlled, long-term Ag^+ delivery.

Systemic drug administration is often ineffective postsurgery or implantation due to impaired blood circulation and insufficient antibiotic concentrations at the affected site. Local delivery systems releasing metallic ions (e.g., Ag^+) or biomolecules (e.g., antibacterial peptides) are effective at maintaining high local concentrations of bioactive agents. They allow for controlled release, thereby lowering the cytotoxicity associated with burst delivery. Moreover, the widespread use of antibiotics has contributed to the emergence of resistant bacterial strains, which are now considered a global health threat. Thus, alternative antibacterial strategies are urgently needed.[28]

The Ti-MOF NH_2-MIL-125(Ti) was synthesized via a solvothermal method (Figure 1a and the Experimental part) and consists of disklike particles, 550−1250 nm in diameter (avg. 824 ± 153 nm) and 327 ± 63 nm thick. This morphology reflects the typical Ti−oxo-cluster-based MOF growth of prior reports on NH_2-MIL-125(Ti). Its uniform, submicrometer size maximizes surface exposure and area.

While Ti−oxo-cluster-based MOFs offer structural advantages, their application in aqueous environments is limited by framework degradation, primarily due to ligand hydrolysis and displacement processes, where water either competes with the organic linker for coordination or breaks Ti−ligand bonds through OH^- attack at the metal centers.[22] This instability is critical during release but is also evident during Ag functionalization, where prolonged exposure to the precursor aqueous solution leads to structural collapse (Figure S1). Annealing in air at 250 °C for 24 h (Ti-MOF-Ann) reinforces Ti−ligand coordination by removing residual solvent and adsorbed species while preserving the MOFs' morphology. This treatment prevents premature degradation, ensuring consistent Ag loading and sustained-release performance.

Following stabilization, Ag functionalization was performed via reactive deposition (3 h of immersion in 100 mM $AgNO_3$, dark conditions). Scanning electron microscopy (SEM; Figure 1b,c) shows unchanged morphology, with no visible Ag nanoparticles, suggesting uniform (framework-level) Ag incorporation. Energy-dispersive spectroscopy (EDS) spectra confirm the presence of Ag (Figure 1d), and the Al signal originates from the substrate (Al used for SEM sample preparation).

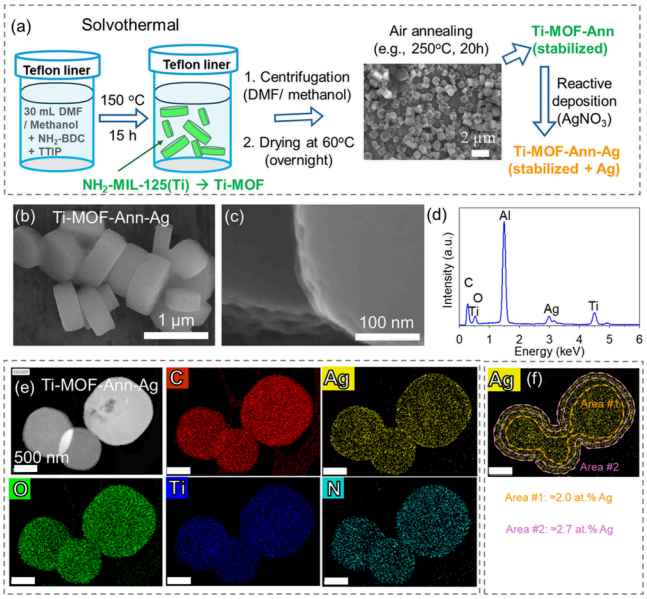

Figure 1. (a) Schematic representation of the synthesis of Ti-MOF [NH_2-MIL-125(Ti)] and its modification with Ag ions. (b and c) High-resolution SEM images of the stabilized and Ag-functionalized MOFs (Ti-MOF-Ann-Ag) with (d) the corresponding EDS spectra. (e) HAADF-STEM image of Ti-MOF-Ann with Ag functionalization and the corresponding EDS elemental mapping images of C, N, O, Ti, and Ag. (f) Ag-EDS profiles of Area #1 (inside the Ag-MOFs) and Area #2 (outer part of the Ag-MOFs). Scale bar of images and f: 500 nm.

High-angle annular dark-field scanning transmission electron microscopy (HAADF-STEM) imaging and EDS mapping (Figure 1e) confirm a uniform distribution of C, N, O, Ti, and Ag throughout the framework, with a Ag content of 2.35 atom % (14.74 wt %). Ag functionalization is on the surface but also in the MOF inner area. Local EDS measurements indicate 2.6 atom % Ag for the outer edges and 2.0 atom % in the inner areas (Figures 1f and S2), a distribution consistent across particles (Figure S3). This internal incorporation supports a diffusion-governed release mechanism and sets this material apart from those relying on surface-deposited Ag nanoparticles (Ag^0).

Thermogravimetric analysis (TGA; Figure 2a) reveals that the Ti-MOF remains thermally stable up to ∼280 °C, with mass loss from physiosorbed water or residual solvent. A pronounced weight loss between 280 and 500 °C reflects the linker's decomposition, while heating above 500 °C results in TiO_2. These results confirm that annealing at 250 °C, below the degradation threshold, preserves structural integrity, aligning with prior Ti−oxo cluster MOF reports,[14,16,29,30] justifying the selected thermal stabilization. Considering the small weight loss between 125 and 270 °C (from 70.5 to 69.5 wt %), such a temperature range would prove optimal. X-ray diffraction (XRD) analysis (Figure 2b) confirms that annealing at 250 °C retains the Ti-MOF crystallinity, whereas 300 °C causes structural collapse and phase transition to TiO_2.[15] More importantly, this occurs hand-in-hand with a Brunauer−Emmett−Teller surface area decrease,[15,30] which confirms the loss of porosity. In our case, up to 250 °C, 24 h, we observe no distinguishable changes in the MOFs' morphology (Figures 2c,d and S4a,b); however, further increasing the time or temperature leads to a smoother morphology and small defects (Figures 2e,f and S4c,d).

https://doi.org/10.1021/acs.nanolett.5c02681
Nano Lett. 2025, 25, 12547−12553

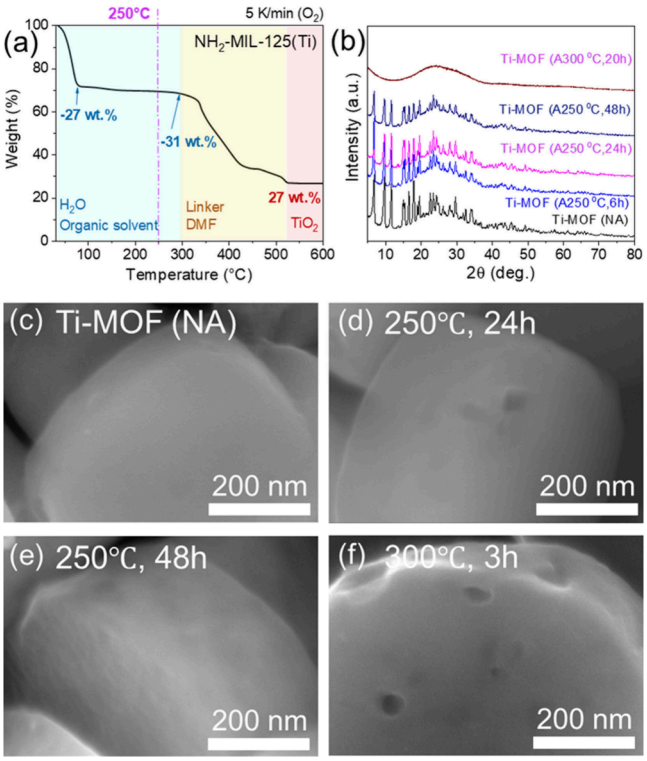

Figure 2. (a) TGA of the Ti-MOF NH_2-MIL-125(Ti) with its initial and final masses (%) after thermal decomposition. (b) XRD graphs for as-prepared [Ti-MOF (NA)] and thermally treated Ti-MOFs (for the indicated temperature and time). High-resolution SEM images of the Ti-MOFs: (c) as-prepared and after annealing at (d) 250 °C for 24 h, (e) 250 °C for 48 h, and (f) 300 °C for 3 h.

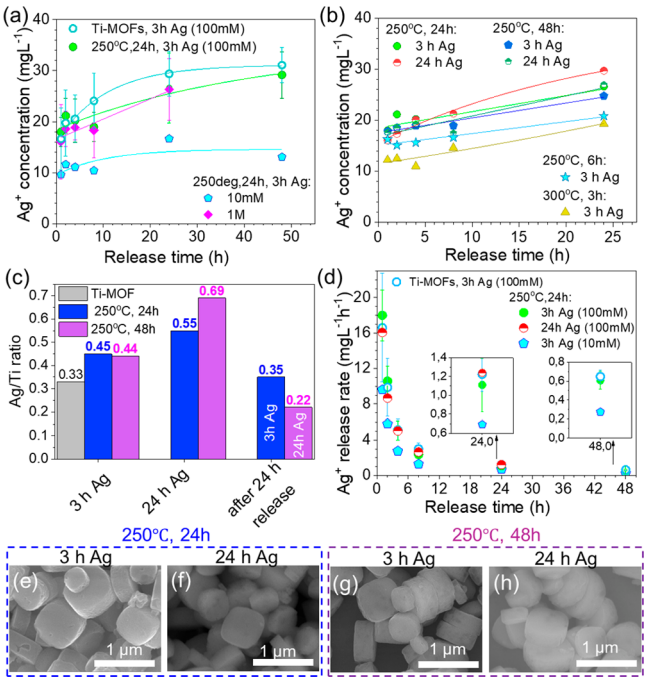

Figure 3. Ag^+ release determined from ion chromatography for (a) Ag-functionalized as-produced MOFs (Ti-MOFs) and MOFs annealed at 250 °C for 24 h (the latter also with different precursor concentrations), and (b) annealed MOFs at 250 °C for different times and 300 °C for 3 h (all samples were functionalized with a 100 mM Ag precursor for the indicated time, 3 or 24 h Ag). (c) Ag loading as a Ag/Ti ratio obtained from EDS for as-produced MOFs and annealed at 250 °C for 24 or 48 h, with different Ag loading times in a 100 mM precursor (3 or 24 h) and also for selected samples after 24 h release in water. (d) Ag^+ release rates for selected samples. SEM images of the annealed and Ag-functionalized MOFs (100 mM, 3 h): (e and f) annealed at 250 °C for 24 h and functionalized for 3 or 24 h, respectively; (g and h annealed at 250 °C for 48 h and functionalized for 3 or 24 h, respectively.

Ion chromatography measurements reveal that thermally stabilized Ag-MOFs exhibit a hybrid two-phase Ag^+ release profile: a moderate initial release (0−6 h) and then diffusion-driven delivery to 48 h and beyond (Figure 3a). This reflects the sequential desorption of loosely coordinated Ag^+ at the MOF surface, followed by the gradual diffusion of ions from internal coordination sites. Moreover, as-prepared MOFs subjected to extended Ag loading times exhibit burst release and degradation, a consequence of their aqueous instability (Figure S5). The optimized conditions (250 °C, 24 h; 100 mM Ag, 3 h) offer a sustained, diffusion-limited delivery over extended periods.

To contextualize our system, we compare it to key Ag-MOF systems. Ag(I)-MOFs as $[Ag_2(O\text{-}IPA)]$ and $[Ag_5(PYDC)_2(OH)]$[23] show promising biocompatibility but require complex multidentate ligands and release Ag^+ slowly. Heteroleptic systems such as Ag-PTA-pma[24] offer multifunctionality (antifungal and anticancer effects) but have limited scalability. Simpler structures, $[Ag_2(BDC)]_n$,[25] improve stability yet lack tunable release. Composites enhance antibacterial activity through near-IR or redox activation (Ag@MOF@PDA[26] and Ag/AgBr-loaded MOFs[27]) but may suffer from ambiguous Ag speciation and rapid depletion. Our approach offers sustained Ag^+ delivery without external triggers or surface-bound particles, addressing both the scalability and mechanistic control.

To elucidate the Ag^+ release mechanism, selected Ag^+ release profiles were fitted with the Korsmeyer−Peppas model (Figure S6). Both Ag-MOF and thermally stabilized MOF-Ann-Ag (100 mM $AgNO_3$, 3 h) showed high correlation coefficients ($R^2 = 0.992$ and 0.898, respectively) and low exponents ($n = 0.16$ and 0.12, respectively), indicating pseudo-Fickian diffusion. These low n values, although below the range of the model, are consistent with constrained ion transport due to surface desorption and limited internal mobility. Lack of convergence with the Higuchi model further supports a nonmatrix diffusion release. In contrast, for the immobilized MOF-Ann-Ag on FTO, the Ag^+ release profile (Figure S7) fits both the Korsmeyer−Peppas ($R^2 = 0.997$ and $n = 0.45$) and Higuchi ($R^2 = 0.969$) models, suggesting a more homogeneous, diffusion-dominated release in coatings. These findings reflect the distinct release dynamics between particulate and coated MOFs, with coatings offering kinetically more consistent Ag^+ delivery.

The Ag^+ concentrations observed (~10−20 mg·L^{-1} over 24−48 h) exceed reported minimum inhibitory concentration values for *E. coli* and *Klebsiella pneumoniae* (5−10 mg·L^{-1}) and approach lower cytotoxic thresholds in mammalian cells (beginning at ~10 mg·L^{-1}[10,31]). This emphasizes the need for dose control, particularly where short-term, localized delivery can be bactericidal, yet within the tolerable window, and the Ag^+ content can be modulated from the functionalization procedure (lower Ag precursor concentration) or by decreasing the amount of applied MOF per unit volume.

https://doi.org/10.1021/acs.nanolett.5c02681
Nano Lett. 2025, 25, 12547−12553

The Ag ion release kinetics were adjusted by varying the precursor concentration (Figure 3a) and annealing conditions (Figure 3b). Functionalization with 100 mM $AgNO_3$ for 3 h provided robust and reproducible release, with proportionally reduced Ag ion uptake and release for lower concentrations (10 mM), whereas higher concentrations (1 M) did not proportionally increase the uptake. Annealing for 48 h (vs 24 h) had a minimal effect for similar Ag functionalization, indicating saturation in the solvent removal during annealing. However, 300 °C annealing (6 h) reduced the ion release due to porosity loss[15,30] and lower loading.

To further assess the Ag incorporation, Ag/Ti atomic ratios were measured for various MOFs (Figure 3c). Annealed samples (250 °C, 24 or 48 h) exhibited higher ratios than as-prepared MOFs under identical functionalization (100 mM $AgNO_3$, 3 h), confirming improved uptake. Longer Ag loading (24 h), particularly in 48-h-annealed MOFs, further increased the content but may compromise the stability. To assess release dynamics, Ag^+ release rates ($mg{\cdot}L^{-1}{\cdot}h^{-1}$) were computed (Figure 3d), showing higher rates in the first 6 h, followed by a diffusion-limited phase, and decreased rates at 24 and 48 h (~1.1 and ~0.6 $mg{\cdot}L^{-1}{\cdot}h^{-1}$, for nonannealed and stabilized 100 mM Ag MOF, respectively). Lower precursor concentrations (10 mM) lead to lower release values, while longer loading times had a minimal effect. Overall, these data support thermal stabilization for sustained Ag^+ delivery.

The stabilized and Ag-functionalized MOF showed no morphological changes in the SEM images (Figure 3e–h). For the optimized MOF (250 °C, 24 h) with 100 mM Ag, 3 h, EDS after 24-h-release experiments revealed that 77% of the initial Ag remains, highlighting the framework's capacity to stably retain Ag^+ and resist leaching. This retention reflects a strong internal coordination and thermal stability, distinguishing it from carriers prone to early depletion. Because cumulative release could not be derived (powder samples were analyzed independently for each time point), the profiles were consistent across replication and align with the retained Ag content observed via EDS, providing a reliable basis for kinetic interpretation.

High-resolution X-ray photoelectron spectroscopy (XPS) spectra (Figure 4) reveal the chemical state of Ag in functionalized MOFs. The spectra for C 1s (at 284.4 eV, CO bonds at 288.5 eV), Ti 2p (458.5 eV), O 1s (530.4 eV), and N 1s (399.0 eV) (Figure 4a–d) show no significant shifts after annealing or Ag loading, confirming that the MOF backbone remains chemically intact (for survey spectra, see Figure S8). Annealing slightly increases the C peak intensity (also due to XPS's surface sensitivity), and Ag incorporation affects the surface reorganization of ligands visible in O 1s, reducing Ti–O and increasing the C=O intensity. Ag 3d spectra (Figure 4e,f) confirm the incorporation of two chemically distinct Ag species. The broad full width at half-maximum (≈2.2 eV), typically ≈1.2 eV,[32] and shoulders at lower binding energies[32] indicate a δ^+ state and metallic Ag (Ag^0). The former is likely by Ag–O coordination (exchanging the C=O, hydroxyl groups, and Ti–oxo clusters) or Ag–N interaction (N and Ag atom interaction, $-NH=^+$ at 399.47 eV).[33]

These findings align with prior reports of partial Ag^+ reduction by hydroxyl and amino groups in aqueous environments,[33,34] as well as Ag–ligand exchange within NH_2-MIL-125(Ti).[33] Alongside the TEM/EDS results (Figures 1, S2, S3, and S9), the XPS data confirm that Ag is

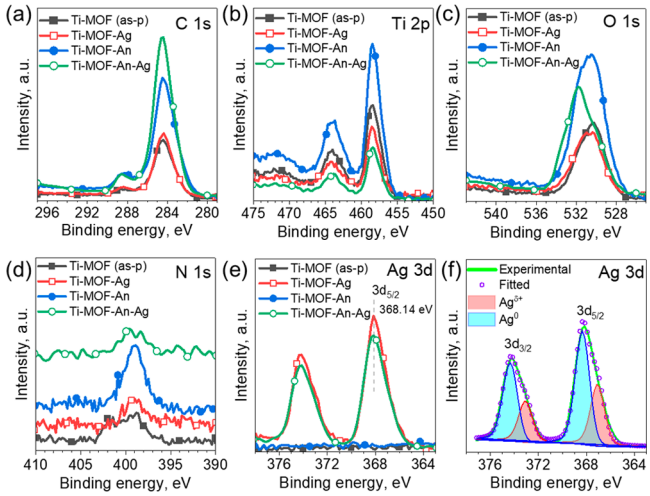

Figure 4. High-resolution XPS data for bare MOFs, Ti-MOF (as-p), and stabilized MOFs at 250 °C for 24 h (Ti-MOF-An) and their Ag-functionalized counterparts, Ti-MOF-Ag and Ti-MOF-An-Ag (functionalization was performed in a 100 mM Ag precursor solution for 3 h): (a) C 1s, (b) Ti 2p, (c) O 1s, (d) N 1s, (e) Ag 3d and (f) corresponding Ag 3d peak fit for the Ag-functionalized annealed MOF (Ti-MOF-An-Ag).

predominantly incorporated as δ^+, with a minor reduced fraction (possibly formed during air exposure postsynthesis), supporting a dual-mode Ag^+ release via framework-coordinated Ag^+ and minor reduced Ag^0.

The therapeutic efficacy of Ag-based systems relies on balancing the ion release rate and retention. Rapid Ag^+ release may exhibit strong initial antibacterial effects but quickly lose potency and risk cytotoxicity. Conversely, overly retentive systems may fail to deliver bactericidal levels. The thermal stabilization strategy employed here enables controlled Ag speciation and diffusion kinetics, making MOFs an adaptable platform. Optimized conditions (250 °C, 24 h; 100 mM Ag, 3 h) ensure sufficient initial release for rapid bacteriostasis and sustained delivery, which is ideal for coatings on implants or wound dressings.

The antibacterial activity of bare and Ag-functionalized MOF powders was evaluated by bacterial kinetics (optical density measurements, OD) and bacterial inhibition (halo formation in agar diffusion tests) against *E. coli* (Figure 5). The OD_{600nm} measurements (Figure 5a) start at a 0.5 bacterial concentration and revealed dose-dependent bacterial inhibition. The 2 mg Ag-MOF sample showed the most pronounced bacteriostatic effect (bacterial growth is decreased and impaired), while the 1 and 0.5 mg samples had an intermediate inhibitory effect that decreases with the decreasing amount of Ag-MOF used (with 0.5 mg not being effective after 24 h). These trends highlight the antimicrobial efficacy of released Ag^+, which disrupts bacterial cellular processes and inhibits metabolic activity.

Agar diffusion assays (Figures 5b and S10) confirmed the dose-dependent antibacterial activity of the optimized Ag-MOFs. Inhibition halos were visible around all Ag-functionalized samples, with the 2 mg sample producing the largest halos. The 1 and 0.5 mg samples exhibited progressively smaller halos, consistent with a reduced Ag^+ release and availability. Bare MOF produced no inhibition zone, confirming the absence of inherent antibacterial properties. After 5 days of incubation (Figure 5c), the 2 mg Ag-MOF still

https://doi.org/10.1021/acs.nanolett.5c02681
Nano Lett. 2025, 25, 12547–12553

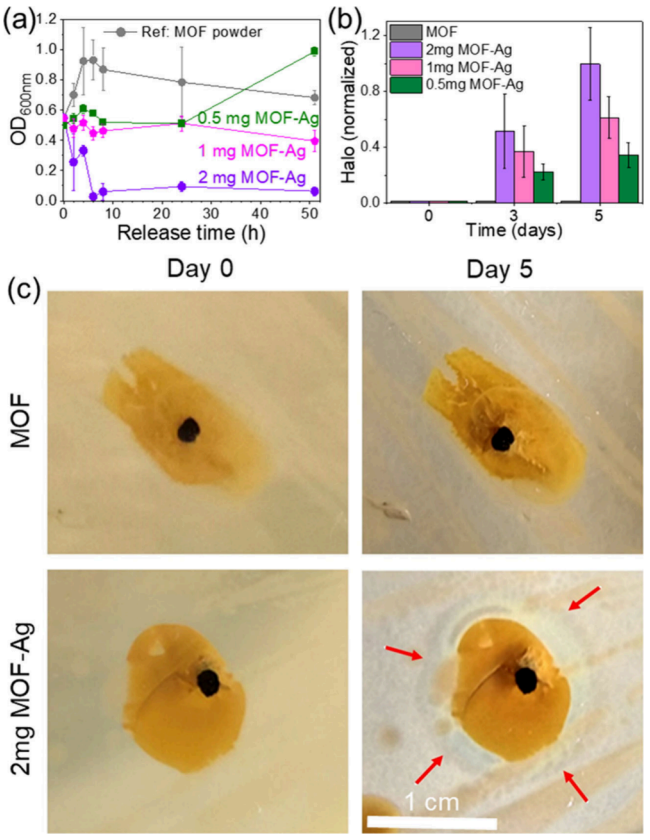

Figure 5. Antibacterial activity of thermally stabilized bare MOFs (2 mg) and Ag-functionalized MOFs (100 mM, 3 h) with different amounts (2, 1, or 0.5 mg): (a) optical density (OD_{600nm}) measurements; (b) antibacterial inhibition halo data for all samples at days 0, 3, and 5; (c) representative optical images of MOF and 2 mg Ag-MOF samples at days 0 and 5 (plate A; scale bar, 1 cm). Tests were performed three times for each condition and time point.

maintained a well-defined halo, demonstrating prolonged Ag^+-mediated bacterial inhibition.

Such Ag-MOFs retain antibacterial efficacy when processed into coatings on FTO substrates. The coatings sustain Ag^+ release over 48 h, exceeding 10 mg·L^{-1} (Figure S7a), while OD measurements confirm bacteriostatic activity comparable to that of the powder form (Figure S11a). SEM imaging revealed a uniform layer (~8 μm thick; Figure S11b). These findings demonstrate that the Ag-MOF system maintains its structural and antibacterial performance in immobilized formats, validating its potential for surface-integrated applications.

These results align with earlier studies showing that Ag^+ release enhances biomaterial antibacterial activity.[5,6,17] In our system, Ag is predominantly incorporated as coordinated Ag^+ within the MOF, and antibacterial effects correlate with the Ag content. Powder forms exhibit a controlled burst followed by sustained release, whereas coatings enable a more gradual delivery, reflecting morphology-driven kinetics. This dual behavior allows tuning for specific applications, providing either rapid bacteriostasis or extended release for long-term protection. Overall, Ag-NH_2-MIL-125(Ti) is a promising platform for antibacterial strategies in coatings, wound interfaces, or other biomedical contexts where controlled Ag ion delivery is critical.

This study demonstrates that thermally stabilized NH_2-MIL-125(Ti) enables uniform Ag incorporation and sustained Ag^+ release from a structurally robust MOF matrix. Annealing at 250 °C enhances aqueous stability, yielding a hybrid release profile: a moderate initial release (first 6 h), followed by diffusion-limited delivery extending beyond 48 h. Over 77% of Ag remains framework-bound after 24 h, confirming strong retention and long-term reservoir behavior.

Compared with conventional Ag-TiO_2 systems, this Ag-MOF platform exhibits higher Ag loading, improved structural stability, and tunable Ag^+ release. STEM/EDS and XPS confirm homogeneous Ag distribution and the absence of agglomeration, supporting a framework-embedded, ion-specific release pathway. Antibacterial assays in both powder and coating formats show dose-dependent efficacy and emphasize how immobilization alters release dynamics.

While further optimization of the coating format (e.g., layer thickness, dosing, or spray-deposition strategies) remains to be explored, these findings establish Ag-NH_2-MIL-125(Ti) as a scalable, format-flexible platform for sustained Ag^+ delivery. Release profiles can be tuned by adjusting the concentration of the Ag precursor used or the MOF loading amount, enabling application in antibacterial coatings, wound interfaces, and implantable surfaces requiring controlled, long-acting antimicrobial activity.[28]

■ ASSOCIATED CONTENT

Supporting Information

The Supporting Information is available free of charge at https://pubs.acs.org/doi/10.1021/acs.nanolett.5c02681.

Experimental part, SEM images of Ti-MOF [NH_2-MIL-125(Ti)], EDS data from inside the Ag-MOFs and the outer part of the Ag-MOFs, HAADF-TEM image and schematic on Ti/Ag EDS maps, annealing effect on the Ti-MOF morphology, Ag release from as-prepared Ti-MOFs upon functionalization by reactive deposition, Korsmeyer−Peppas/Highuchi fits for selected Ag-MOFs in powder or coating form, survey XPS spectra of bare and stabilized MOFs, HAADF-TEM image of Ti-MOF annealed with Ag functionalization, optical images of agar plates on days 0, 3, and 5, and antibacterial activity and SEM images of Ag-MOF layers measured by optical density (OD = 600 nm) (PDF)

■ AUTHOR INFORMATION

Corresponding Authors

Anca Mazare − *Department of Materials Science, Institute for Surface Science and Corrosion, Friedrich-Alexander-Universität Erlangen−Nürnberg (FAU), Erlangen 91058, Germany;* orcid.org/0000-0002-4836-946X; Email: anca.mazare@fau.de

Patrik Schmuki − *Department of Materials Science, Institute for Surface Science and Corrosion, Friedrich-Alexander-Universität Erlangen−Nürnberg (FAU), Erlangen 91058, Germany; Regional Centre of Advanced Technologies and Materials, Olomouc 78371, Czech Republic;* orcid.org/0000-0002-9208-5771; Email: schmuki@ww.uni-erlangen.de

Authors

Wolfgang H. Goldmann − *Department of Physics, Chair of Biophysics, Friedrich-Alexander-Universität Erlangen−Nürnberg (FAU), Erlangen 91052, Germany;* orcid.org/0000-0003-0738-2665

https://doi.org/10.1021/acs.nanolett.5c02681
Nano Lett. 2025, 25, 12547−12553

Esra Kocak − *Department of Materials Science, Institute for Surface Science and Corrosion, Friedrich-Alexander-Universität Erlangen−Nürnberg (FAU), Erlangen 91058, Germany; Department of Molecular Biology and Genetics, İzmir Institute of Technology, Urla 35430 İzmir, Turkey*

Benedict Osuagwu − *Department of Materials Science, Institute for Surface Science and Corrosion, Friedrich-Alexander-Universität Erlangen−Nürnberg (FAU), Erlangen 91058, Germany*

Shanshan Qin − *Department of Materials Science, Institute for Surface Science and Corrosion, Friedrich-Alexander-Universität Erlangen−Nürnberg (FAU), Erlangen 91058, Germany;* orcid.org/0000-0001-7693-115X

Ran Cao − *State Key Laboratory of Advanced Fiber Materials, College of Materials Science and Engineering, Donghua University, Shanghai 201620, China*

Complete contact information is available at: https://pubs.acs.org/10.1021/acs.nanolett.5c02681

Author Contributions

†A.M., W.H.G., and E.K. contributed equally to this work. E.K., B.O., S.Q., and R.C. optimized the MOF synthesis. E.K. and B.O. stabilized/functionalized the MOFs. W.H.G. and A.M. performed the antibacterial experiments. A.M. performed the surface analytics experiments. A.M. and P.S. supervised the project. A.M. handled initial draft and revision (with comments from all authors). The manuscript was written through contributions of all authors. All authors have given approval to the final version of the manuscript.

Notes

The authors declare no competing financial interest.

■ ACKNOWLEDGMENTS

W.H.G. thanks the Deutsche Forschungsgemeinschaft (DFG) (Grant 540989797) for financial support. E.K. thanks the Erasmus+ Student Mobility for Traineeships for funding. The authors thank the Center for Nanoanalysis and Electron Microscopy (FAU) and Tadahiro Yokosawa for performing the TEM measurements. Rainer Illmann is thanked for the ion chromatography measurements. The Institute of Polymer Materials (LSP, FAU) and Jennifer Reiser are thanked for the TGA measurements.

■ REFERENCES

(1) Lee, K.; Mazare, A.; Schmuki, P. One-Dimensional Titanium Dioxide Nanomaterials: Nanotubes. *Chem. Rev.* **2014**, *114*, 9385−9454.

(2) Ion, R.; Necula, M. G.; Mazare, A.; Mitran, V.; Neacsu, P.; Schmuki, P.; Cimpean, A. Drug Delivery Systems Based on Titania Nanotubes and Active Agents for Enhanced Osseointegration of Bone Implants. *Curr. Med. Chem.* **2020**, *27* (6), 854−902.

(3) Chernousova, S.; Epple, M. Silver as Antibacterial Agent: Ion, Nanoparticle, and Metal. *Angew. Chemie Int. Ed.* **2013**, *52* (6), 1636−1653.

(4) Rodrigues, A. S.; Batista, J. G. S.; Rodrigues, M. Á. V.; Thipe, V. C.; Minarini, L. A. R.; Lopes, P. S.; Lugão, A. B. Advances in Silver Nanoparticles: A Comprehensive Review on Their Potential as Antimicrobial Agents and Their Mechanisms of Action Elucidated by Proteomics. *Front. Microbiol.* **2024**, *15*. DOI: 10.3389/fmicb.2024.1440065.

(5) Sabaghian, H. Silver Nanoparticles as Antiviral and Antibacterial Agents: A Comprehensive Review of Synthesis Methods and Therapeutic Application. *ChemistrySelect* **2024**, *9* (12). DOI: 10.1002/slct.202304941.

(6) Marambio-Jones, C.; Hoek, E. M. V. A Review of the Antibacterial Effects of Silver Nanomaterials and Potential Implications for Human Health and the Environment. *J. Nanoparticle Res.* **2010**, *12* (5), 1531−1551.

(7) Anees Ahmad, S.; Sachi Das, S.; Khatoon, A.; Tahir Ansari, M.; Afzal, M.; Saquib Hasnain, M.; Kumar Nayak, A. Bactericidal Activity of Silver Nanoparticles: A Mechanistic Review. *Mater. Sci. Energy Technol.* **2020**, *3*, 756−769.

(8) Molina, J.; Valero-Gómez, A.; Belda, J.; Bosch, F.; Bernabé-Quispe, P.; Tormo-Mas, M. A. Long-Term Antibacterial Ag+-Release Biomaterials Based on Anodized Ti6Al4V and Silver Nanoparticles. *Colloids Surfaces A Physicochem. Eng. Asp.* **2023**, *676*, No. 132243.

(9) Shivaram, A.; Bose, S.; Bandyopadhyay, A. Mechanical Degradation of TiO2 Nanotubes with and without Nanoparticulate Silver Coating. *J. Mech. Behav. Biomed. Mater.* **2016**, *59*, 508−518.

(10) Shivaram, A.; Bose, S.; Bandyopadhyay, A. Understanding Long-Term Silver Release from Surface Modified Porous Titanium Implants. *Acta Biomater.* **2017**, *58*, 550−560.

(11) Bhattacharjee, S. Understanding the Burst Release Phenomenon: Toward Designing Effective Nanoparticulate Drug-Delivery Systems. *Ther. Delivery* **2021**, *12* (1), 21−36.

(12) Onyenso, G.; Vakamulla Raghu, S. N.; Hartwich, P.; Killian, M. S. Modulated-Diameter Zirconia Nanotubes for Controlled Drug Release—Bye to the Burst. *J. Funct. Biomater.* **2025**, *16* (2), 37.

(13) Li, H.; Li, L.; Lin, R.-B.; Zhou, W.; Zhang, Z.; Xiang, S.; Chen, B. Porous Metal-Organic Frameworks for Gas Storage and Separation: Status and Challenges. *EnergyChem.* **2019**, *1* (1), No. 100006.

(14) Castellanos, N. J.; Martinez Rojas, Z.; Camargo, H. A.; Biswas, S.; Granados-Oliveros, G. Congo Red Decomposition by Photocatalytic Formation of Hydroxyl Radicals (·OH) Using Titanium Metal−Organic Frameworks. *Transit. Met. Chem.* **2019**, *44* (1), 77−87.

(15) Alzard, R. H.; Siddig, L. A.; Alhatti, N.; Abdallah, I.; Aljabri, L.; Alblooshi, A.; Alzamly, A. Titania Derived from NH2-MIL-125(Ti) Metal−Organic Framework for Selective Photocatalytic Conversion of CO 2 to Propylene Carbonate. *Comments Inorg. Chem.* **2023**, *43* (1), 1−15.

(16) Andrade, P. H. M.; Dhainaut, J.; Volkringer, C.; Loiseau, T.; Moncomble, A.; Hureau, M.; Moissette, A. Stability of Iodine Species Trapped in Titanium-Based MOFs: MIL-125 and MIL-125_NH 2. *Small* **2024**, *20* (35). DOI: 10.1002/smll.202400265.

(17) Hassan, P. B.; Mohammed Ameen, S. S.; Mohammed, L.; Muhammed Ameen, S. M.; Omer, K. M. Enhanced Antibacterial Activity of a Novel Silver-Based Metal Organic Framework towards Multidrug-Resistant Klebsiella Pneumonia. *Nanoscale Adv.* **2024**, *6* (15), 3801−3808.

(18) Lu, X.; Ye, J.; Zhang, D.; Xie, R.; Bogale, R. F.; Sun, Y.; Zhao, L.; Zhao, Q.; Ning, G. Silver Carboxylate Metal−Organic Frameworks with Highly Antibacterial Activity and Biocompatibility. *J. Inorg. Biochem.* **2014**, *138*, 114−121.

(19) Abánades Lázaro, I.; Chen, X.; Ding, M.; Eskandari, A.; Fairen-Jimenez, D.; Giménez-Marqués, M.; Gref, R.; Lin, W.; Luo, T.; Forgan, R. S. Metal−Organic Frameworks for Biological Applications. *Nat. Rev. Methods Prim.* **2024**, *4* (1), 42.

(20) Abdul Mubarak, N. S.; Foo, K. Y.; Schneider, R.; Abdelhameed, R. M.; Sabar, S. The Chemistry of MIL-125 Based Materials: Structure, Synthesis, Modification Strategies and Photocatalytic Applications. *J. Environ. Chem. Eng.* **2022**, *10* (1), No. 106883.

(21) Zhang, R.; Zhang, W.; Zhu, Q.; Nie, Q.; Zhang, S.; Zhang, Y.; Liu, R.; Liu, Y.; Lin, X.; Li, Y. Engineering Polydopamine-Functionalized NH2-MIL-125 (Ti) for Tetracycline Degradation and Antibacterial Applications. *Surfaces and Interfaces* **2024**, *54*, No. 105188.

(22) Gómez-Avilés, A.; Muelas-Ramos, V.; Bedia, J.; Rodriguez, J. J.; Belver, C. Thermal Post-Treatments to Enhance the Water Stability of NH2-MIL-125(Ti). *Catalysts* **2020**, *10* (6), 603.

(23) Lu, X.; Ye, J.; Zhang, D.; Xie, R.; Bogale, R. F.; Sun, Y.; Zhao, L.; Zhao, Q.; Ning, G. Silver Carboxylate Metal−Organic Frameworks

with Highly Antibacterial Activity and Biocompatibility. *J. Inorg. Biochem.* **2014**, *138*, 114−121.
(24) Jaros, S. W.; Król, J.; Bażanów, B.; Poradowski, D.; Chrószcz, A.; Nesterov, D. S.; Kirillov, A. M.; Smoleński, P. Antiviral, Antibacterial, Antifungal, and Cytotoxic Silver(I) BioMOF Assembled from 1,3,5-Triaza-7-Phoshaadamantane and Pyromellitic Acid. *Molecules* **2020**, *25* (9), 2119.
(25) Paratore, V.; Franco, D.; Guglielmino, S.; Lo Presti, F.; Traina, F.; Conoci, S.; Condorelli, G. G. New Metastable Interfacial Synthesis of a Silver-Terephthalate Metal Organic Framework: Structure, Morphology and Antibacterial Activities. *Mater. Adv.* **2024**, *5* (3), 1033−1044.
(26) He, Y.; Wang, X.; Zhang, C.; Sun, J.; Xu, J.; Li, D. Near-Infrared Light-Mediated Cyclodextrin Metal−Organic Frameworks for Synergistic Antibacterial and Anti-Biofilm Therapies. *Small* **2023**, *19* (35). DOI: 10.1002/smll.202300199.
(27) Wu, D.; Han, L. Fabrication of Novel Ag/AgBr/NH 2 -MIL-125(Ti) Nanocomposites with Enhanced Visible-Light Photocatalytic Activity. *Mater. Res. Express* **2019**, *6* (12), No. 125501.
(28) Goldmann, W. H. Biosensitive and Antibacterial Coatings on Metallic Material for Medical Applications. *Cell Biol. Int.* **2021**, *45* (8), 1624−1632.
(29) Gu, Y.; Cheng, K.; Wu, Y.; Wang, Y.; Morlay, C.; Li, F. Metal−Organic Framework-Templated Synthesis of Bifunctional N-Doped TiO 2 − Carbon Nanotablets via Solid-State Thermolysis. *ACS Sustain. Chem. Eng.* **2016**, *4* (12), 6744−6753.
(30) Hussain, M. Z.; Bahri, M.; Heinz, W. R.; Jia, Q.; Ersen, O.; Kratky, T.; Fischer, R. A.; Zhu, Y.; Xia, Y. An in Situ Investigation of the Thermal Decomposition of Metal-Organic Framework NH2-MIL-125 (Ti). *Microporous Mesoporous Mater.* **2021**, *316*, No. 110957.
(31) Guo, Z.; Chen, C.; Gao, Q.; Li, Y.; Zhang, L. Fabrication of Silver-Incorporated TiO2 Nanotubes and Evaluation on Its Antibacterial Activity. *Mater. Lett.* **2014**, *137*, 464−467.
(32) Ferraria, A. M.; Carapeto, A. P.; Botelho do Rego, A. M. X-Ray Photoelectron Spectroscopy: Silver Salts Revisited. *Vacuum* **2012**, *86* (12), 1988−1991.
(33) Ren, X.; Wang, C.-C.; Li, Y.; Wang, C.-Y.; Wang, P.; Gao, S. Ag(I) Removal and Recovery from Wastewater Adopting NH2-MIL-125 as Efficient Adsorbent: A 3Rs (Reduce, Recycle and Reuse) Approach and Practice. *Chem. Eng. J.* **2022**, *442*, No. 136306.
(34) Lu, Q.; Deng, J.; Hou, Y.; Wang, H.; Li, H.; Zhang, Y.; Yao, S. Hydroxyl-Rich C-Dots Synthesized by a One-Pot Method and Their Application in the Preparation of Noble Metal Nanoparticles. *Chem. Commun.* **2015**, *51* (33), 7164−7167.

https://doi.org/10.1021/acs.nanolett.5c02681
Nano Lett. 2025, 25, 12547−12553